

# Photon-Photon Quantum Phase Gate in a Photonic Molecule with $\chi^{(2)}$ Nonlinearity

Ming Li<sup>1,2</sup>, Yan-Lei Zhang,<sup>1,2</sup> Hong X. Tang,<sup>3</sup> Chun-Hua Dong,<sup>1,2,\*</sup> Guang-Can Guo,<sup>1,2</sup> and Chang-Ling Zou<sup>1,2,4,†</sup>

<sup>1</sup>Key Laboratory of Quantum Information, Chinese Academy of Sciences, University of Science and Technology of China, Hefei, 230026 Anhui, People's Republic of China

<sup>2</sup>CAS Center For Excellence in Quantum Information and Quantum Physics, University of Science and Technology of China, Hefei, 230026 Anhui, People's Republic of China

<sup>3</sup>Department of Electrical Engineering, Yale University, New Haven, Connecticut 06511, USA

<sup>4</sup>National Laboratory of Solid State Microstructures, Nanjing University, Nanjing, 210093 Jiangsu, China

(Received 30 September 2019; revised manuscript received 2 March 2020; accepted 23 March 2020; published 6 April 2020)

The construction of a photon-photon quantum phase gate based on photonic nonlinearity has long been a fundamental issue, and is vital for deterministic and scalable photonic quantum-information processing. It requires not only strong nonlinear interaction at the single-photon level but also suppressed phase noise and spectral entanglement for high gate fidelity. In this paper, we propose that a high-quality-factor microcavity with strong  $\chi^{(2)}$  nonlinearity can be quantized to anharmonic energy levels and can be effectively treated as an artificial atom. Such an artificial atom has a size much larger than the photon wavelength, which enables passive and active ultrastrong coupling to traveling photons. A high-fidelity quantum control phase gate is realized by our mediating the phase between photons with an intermediate artificial atom in a photonic molecule structure. The scheme avoids two-photon emission and thus eliminates spectral entanglement and quantum phase noise. Experimental realization of the artificial atom can be envisioned on an integrated photonic chip and holds great potential for single-emitter-free, room-temperature quantum-information processing.

DOI: 10.1103/PhysRevApplied.13.044013

## I. INTRODUCTION

The quantum photonic integrated circuit (PIC) has been extensively studied in the last decade for photon-based quantum-information processing [1–5] due to its advantages of stability, compactness, and low power consumption. Essential quantum optical components, including quantum photon sources [6], quantum gates [7,8], and single-photon detectors [9–11], have all been demonstrated on the PIC with excellent performances, and a fully integrated quantum PIC is within reach [12]. However, the absence of single-photon nonlinearity greatly limits the development of a PIC for scalable quantum processors [13]. It is believed that the intrinsic nonlinear effect of a dielectric is too weak compared with the material absorption [13], and thus the desired quantum operation cannot be accomplished before the photon is lost. As a result, photonic two-qubit quantum gates are implemented probabilistically with pure linear optical components and rely on quantum interference and ancillary photons [7,14].

Another approach to overcome this obstacle involves introducing single emitters into the PIC, but this suffers from the experimental challenges of nanomanipulation and instabilities of emitters [15–17].

Fortunately, recent exciting progress in nonlinear optics on the PIC has encouraged efforts to pursue nonlinearity at the single-photon level by realizing microresonators and nanoresonators of ultrahigh quality factor and ultrasmall mode volume [18–21]. In the past few years, cavity-enhanced nonlinear photonics has achieved great success in frequency conversion, frequency comb, and quantum photon sources [19,22–25]. Especially, ultrahigh-efficiency second-harmonic generation (SHG) with efficiency as high as 10<sup>6</sup>%/W has been achieved [26–29]. All this exciting progress achieved with  $\chi^{(2)}$  nonlinearity, such as in lithium niobate (LN) [29–32], (AlN) [26,33], and gallium arsenide (GaAs) [27], indicates a saturation of conversion efficiency even at single-photon-level pump, and reveals a promising path toward single-photon-level nonlinearity. When the single-photon coupling strength approaches the cavity dissipation rate, the vacuum strong-coupling regime is reached, and the bare cavity without external driving shows photon energy levels with strong

\*chunhua@ustc.edu.cn

†clzou321@ustc.edu.cn

anharmonicity. It was anticipated that the atomlike nature of a cavity with strong  $\chi^{(2)}$  and  $\chi^{(3)}$  nonlinearity could find applications in single-photon sources by photon blockade [34–36].

However, there is still another obstacle for deterministic photonic quantum gates, since they demand the processing of the photon's quantum states while maintaining the spectral-temporal wave function. As pointed out by Shapiro *et al.* [37–40], the fidelity of a photon-photon quantum gate based on photonic nonlinearity, such as the Kerr effect, suffers from spectral entanglement and phase noise, due to the spatially local interaction and multimode nature of traveling photons in the frequency domain. Even though several schemes have been proposed to overcome such a limitation by introducing nonlocal interaction, the quantum Zeno blockade effect, and cascaded sites [41–46], these studies are still based on propagation modes and the intrinsic optical loss in nonlinear media is not considered.

In this work, we propose an artificial atom on a PIC by using  $\chi^{(2)}$  nonlinearity in a well-engineered microresonator. The artificial atom has a size of microns, and thus is easy to use for strong coupling with a waveguide, which enables efficient quantum storage and extraction of photons. As an example, we proposed an architecture for realizing a quantum controlled-Z (CZ) gate based on a photonic molecule [31], breaking the limitations of the spatially-local-interaction condition for traveling photons, thus being immune from spectral entanglement and phase noise. With potentially achievable parameters in the experiment, we predict a fidelity of the CZ gate of 99%. Combining the CZ gate with the mature (Hadamard and phase gates) by linear optical elements, the universal-quantum-gate set [47] can be accomplished and scalable quantum computation is promising on the PIC platform.

## II. ARTIFICIAL ATOM

Figure 1(a) schematically illustrates the artificial atom, which is based on a phase-matched  $\chi^{(2)}$  ultrahigh- $Q$  microresonator. By careful design of the geometry dispersion of the cavity, certain modes that fulfill the phase-matching condition for nonlinear interaction can be realized. For example, the highly efficient second-harmonic generation between modes in the visible and near-infrared bands have been experimentally demonstrated with AlN, LN, and GaAs microrings [26,27,29,33]. For nonlinearly coupled optical modes, the system Hamiltonian reads [23,26] ( $\hbar = 1$ )

$$H_{AA} = \sum_j \omega_j j^\dagger j + g_d (a^{\dagger 2} c + a^2 c^\dagger), \quad (1)$$

where  $j \in \{a, c\}$  represents the resonant modes of the cavity and the mode frequency  $2\omega_a \approx \omega_c$  for a degenerate three-wave mixing process. For the nondegenerate

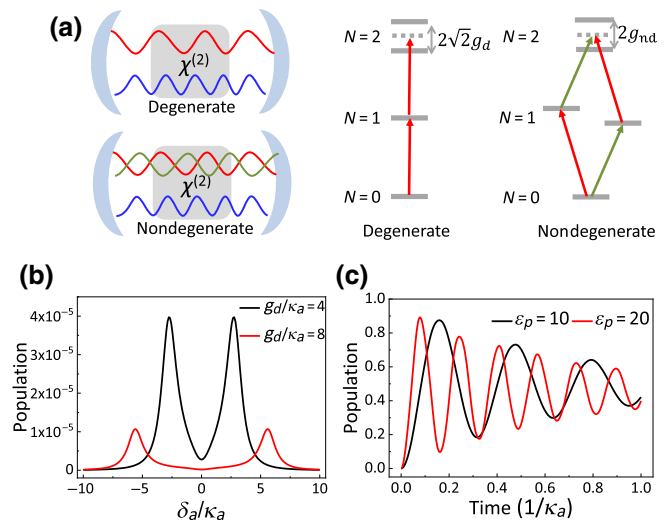


FIG. 1. Artificial atom based on an optical cavity with strong  $\chi^{(2)}$  nonlinearity. (a) Left: degenerate and nondegenerate three-wave mixing, corresponding to SHG and sum-frequency generation. Right: energy-level structures for  $\chi^{(2)}$  interaction. (b) Vacuum Rabi splitting of the populations of state  $|2_a 0_c\rangle$  for SHG. The black curve corresponds to  $g_d/\kappa_a = 4$  and the red curve corresponds to  $g_d/\kappa_a = 8$ . The driving strength  $\varepsilon_p = 0.2$ . (c) Rabi oscillation of the single-photon-excitation state  $|1_a 0_c\rangle$  population under coherent driving. The black curve corresponds to  $\varepsilon_p = 10$  and red curve corresponds to  $\varepsilon_p = 20$ . The coupling strength  $g_d/\kappa_a = 80$ . The cavity decay rates are set at  $\kappa_a = \kappa_c = 1$ .

case  $j \in \{a, b, c\}$ , the interaction reads  $g_{nd} (a^\dagger b^\dagger c + abc^\dagger)$ , with  $\omega_a \neq \omega_b$  and  $\omega_b \approx \omega_c - \omega_a$ . Here  $a, b, c$  denotes the bosonic operator for the modes, and  $g_d, g_{nd} \propto \chi^{(2)} \xi / \sqrt{V}$  is the coupling strength, which is determined by the modal overlap  $\xi$ , cavity mode volume  $V$ , and the material nonlinear susceptibility  $\chi^{(2)}$ .

In conventional bulk nonlinear optics, the coupling rate is much less than the dissipation rate due to large  $V$  (i.e.,  $g \ll \kappa_j$ , with dissipation rate  $\kappa_j = \omega_j / 2Q_j$ , where  $Q_j$  is the corresponding cavity quality factor). Thus, the conversion from  $a, b$  to  $c$  occurs only by strong pumping of the system [23,26]. With increased  $\xi$  and drastically reduced  $V$  in the PIC,  $g$  increases and approaches  $\kappa$ , and thereby the quantum effect appears, as shown in the right panel in Fig. 1(a). Considering only few excitations in those modes, the system energy levels can be rewritten as  $|l_a n_c\rangle$  or  $|l_a m_b n_c\rangle$  in the Fock-state basis, with  $l, m, n \in \mathbb{Z}$  (the subscripts of the states are omitted in the following). Because of the nonlinear interaction in degenerate case, the energy levels  $|20\rangle$  and  $|01\rangle$  are hybridized and produce eigenstates  $(|20\rangle \pm |01\rangle)/\sqrt{2}$ , whose energy levels are shifted by  $+\sqrt{2}g_d$  and  $-\sqrt{2}g_d$ , respectively. Similarly, for the nondegenerate case, the state  $|110\rangle$  strongly couples with  $|001\rangle$  and produces new eigenstates  $(|110\rangle \pm |001\rangle)/\sqrt{2}$  with frequency splitting  $2g_{nd}$ . Then, the cavity shows anharmonicity for Fock states of modes  $a$  (or  $a$  and  $b$ ),

as shown by the dashed lines in Fig. 1(a). When  $\kappa < g_d, g_{nd}$ , the states with excitation number  $N \geq 2$  are no longer resonant with the bare cavity, which will lead to the photon-blockade effect [35,36,48]. In this case, we treat the cavity as an artificial atom. It is worth noting that the artificial atom based on the anharmonicity of Fock states shares the same spirit of a superconducting qubit [49], which is an  $LC$  circuit with strong anharmonicity and is usually treated as a two-level system.

To verify the artificial atom, a weak coherent driving  $\varepsilon_p (a^\dagger + a)$  is used to probe the system with  $g_d/\kappa_a = 4$  or 8 for the degenerate case. The numerical simulation is performed with QUANTUM TOOLBOX IN PYTHON [50]. Figure 1(b) shows the dependence of the  $|20\rangle$ -state population on the frequency of a continuous driving field ( $\varepsilon_p = 0.2$ ). The population at zero detunings is greatly suppressed due to the splitting of the hybrid energy levels. Furthermore, the temporal behavior of the artificial atom under on-resonance driving shows clear Rabi oscillation [Fig. 1(c)], since only  $|00\rangle$  and  $|10\rangle$  can be effectively excited, thus confirming the equivalence of our system to a two-level atom. The blockade effect on the high-excitation energy levels can be used to build a deterministic single-photon source.

It is worth noting that the vacuum Rabi splitting shown in Fig. 1(b) is essentially distinct from the recently demonstrated all-optical strong coupling in a  $\chi^{(2)}$  microring [23]. Our scheme here requires the vacuum coupling strength  $g > \kappa_j$ , which manifests itself as vacuum strong coupling, in contrast to the coupling strength  $\sqrt{N_{\text{pump}}}g > \kappa_j$  stimulated by the intracavity pump photon number ( $N_{\text{pump}}$ ) in Ref. [23]. The result of vacuum strong coupling similar to that in Fig. 1(b) was also studied by Irvine *et al.* [34], in which the possible schemes, including better engineering of the cavity or use of a coherent pump to stimulate the coupling, to observe the strong coupling effect are discussed. However, here we focus on the quantum effects arising in the cavity due to the anharmonicity. For example, the Rabi oscillation due to a continuous external driving in Fig. 1(c) indicates the quantum nature of the artificial atom, and also indicates the manipulation of the internal state of the artificial atom by a laser.

Compared with natural atoms, the artificial atom maintains many advantages of photonic cavities. Firstly, degenerate clockwise and counterclockwise modes are supported in a traveling-wave microresonator. Therefore, the artificial atom can couple with external photons unidirectionally [Fig. 2(a)], which is possible only for natural atoms with photonic spin-orbit coupling [51]. Especially, the twofold degeneracy of modes enables the construction of two identical artificial atoms with only one design, offering more energy levels for quantum-information processing. Secondly, the artificial atoms are more flexible for photonic structure designs and allow highly efficient coupling with a waveguide or other photonic structures. In previous studies

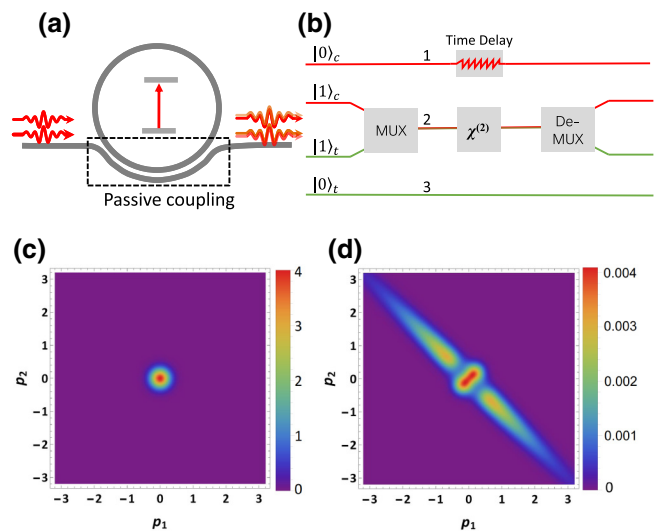


FIG. 2. Coupling between a waveguide and an artificial atom made by a microring cavity. (a) The artificial atom is coupled with a waveguide with a wrapped-around structure. The coupling rate can be 3 orders of magnitude greater than the decay rate. (b) Dual-rail encoding scheme for a quantum gate of two propagating photons. The two photons are multiplexed into the same waveguide and interact with each other in the  $\chi^{(2)}$  medium and are then demultiplexed to different waveguides. A time delay is added in the first path to make  $|0\rangle_c$  and  $|1\rangle_c$  synchronized in the time domain. (c) Input state of a separable two-photon state with Gaussian shape  $\phi_{in}(k_1, k_2) = (1/2\pi\sigma^2) \exp[-(k_1^2 + k_2^2)/2\sigma^2]$ , where  $k_1$  ( $k_2$ ) is the frequency of the photon and  $\sigma = 0.5$  is the width of the frequency distribution. (d) Output state. The nonlinear coupling strength  $g_d = 3$  and the decay rates of the second-harmonic mode  $\kappa_{c,0} = \kappa_{c,1} = 1$  and the fundamental mode  $\kappa_{a,0} = 1, \kappa_{a,1} = 3$ , where  $\kappa_{a,0}$  ( $\kappa_{c,0}$ ) is the intrinsic decay rate and  $\kappa_{a,1}$  ( $\kappa_{c,1}$ ) is the external coupling rate to the waveguide. DEMUX, time-bin demultiplexer; MUX, time-bin multiplexer.

on waveguide quantum electrodynamics [52,53], the cooperative interaction between single emitters and waveguide modes could be described by the Purcell factor, which corresponds to the ratio between the rate of spontaneous emission into the waveguide and the rate of intrinsic emission into free space. Similarly, the Purcell factor for the artificial atom can be calculated as  $F_P = \kappa_1/\kappa_0$ , where the external coupling rate  $\kappa_1$  between the waveguide and the cavity can be tens of gigahertz, while the intrinsic decay rate  $\kappa_0$  of a cavity is on the order of megahertz for intrinsic  $Q \sim 10^7$ . Therefore, an effective Purcell factor  $F_P = \kappa_1/\kappa_0$  exceeding 1000 is achievable by an artificial atom with the configuration in Fig. 2(a). In contrast, the achievable  $F_P$  for natural atom-waveguide coupling is limited to  $\mathcal{O}(1)$ . In addition to the passive design, the interaction between the artificial atom and photons as well as the energy levels could also be dynamically controlled by active antennas via electro-optic (EO) or thermal-optic effects.

### III. CZ-GATE SCHEME

These merits of artificial atoms make them an excellent platform for realizing scalable quantum gates for photons or atoms. By use of the photon-blockade effect in a strongly coupled artificial atom and waveguide, the probe single photon will gain a  $\pi$  phase when passing the artificial atom if its frequency is on resonance with its transition. However, if the photon is off resonance with the transition, the artificial atom will not induce a phase shift. Therefore, it is anticipated that one photon could induce a  $\pi$  phase shift of another photon, manifesting the CZ gate for photons. In this work, we consider the dual-rail encoding of single photons, as shown in Fig. 2(b). When both the control and the target photon enter into same path, the artificial atom can mediate the strong interaction between the photons and thus realize a deterministic controlled-phase gate.

#### A. Two-photon scattering

First, we test the artificial atom by coupling it to a bus waveguide [Fig. 2(a)] with a direct input of two cooperating photons [Fig. 2(c)]. The two-photon wave function evolves to the superposition of a single-photon state in the second-harmonic frequency and a two-photon state in the fundamental frequency during the nonlinear interaction inside the nonlinear cavity. The input-output formalism of the two-photon scattering problem is derived as (see the Appendix for details)

$$\begin{aligned} S(p_1, p_2; k_1, k_2) &= t_{k_1} t_{k_2} (\delta_{p_1, k_1} \delta_{p_1, k_2} + \delta_{p_1, k_2} \delta_{p_2, k_1}) \\ &\quad + \frac{B(k_1, k_2)}{\sqrt{2}\kappa_{a,1}} (2 - t_{p_1} - t_{p_2}) \delta_{p_1+p_2, k_1+k_2}, \end{aligned} \quad (2)$$

$$S(p; k_1, k_2) = C(k_1 + k_2) \delta_{p, k_1+k_2}, \quad (3)$$

where  $S(p_1, p_2; k_1, k_2)$  [ $S(p; k_1, k_2)$ ] is the probability amplitude for two photons with frequencies  $p_1$  and  $p_2$  ( $p$  is the frequency of a single photon in the second-harmonic frequency band) with input photons of frequencies  $k_1$  and  $k_2$ ,  $\delta_{i,j}$  has nonzero value 1 only for  $i = j$ ,  $C(k_1, k_2) = -[2g_d\sqrt{2\kappa_{c,1}}(2 - t_{k_1} - t_{k_2})/\sqrt{\pi}(\xi_a^- \xi_c^- - 2g_d^2)]$ , and  $B(k_1, k_2) = \sqrt{2}g_d^2(1 - t_{k_1})(1 - t_{k_2})/\pi(\xi_a^- \xi_c^- - 2g_d^2)$  where  $t_k = (k - \omega_a + i\kappa_{a,0} - i\kappa_{a,1})/(k - \omega_a + i\kappa_{a,0} + i\kappa_{a,1})$  is the transmittance of the single-photon state,  $\xi_a^\pm = 2(\omega_a - i\kappa_{a,0} \pm i\kappa_{a,1}) - k_1 - k_2$ , and  $\xi_c^\pm = (\omega_c - i\kappa_{c,0} \pm i\kappa_{c,1}) - k_1 - k_2$ , where  $\kappa_{i,0}$  and  $\kappa_{i,1}$  are the intrinsic decay rate and external coupling rate to the waveguide of the  $i$ th mode, respectively. For a separable two-photon input state with a Gaussian shape

$$\phi_{\text{in}}(k_1, k_2) = \frac{1}{2\pi\sigma^2} \exp[-(k_1^2 + k_2^2)/2\sigma^2], \quad (4)$$

the output two-photon state is calculated as

$$\phi_{\text{out}}(k_1, k_2) = \iint dk_1 dk_2 \phi_{\text{in}}(k_1, k_2) S(p_1, p_2; k_1, k_2). \quad (5)$$

The outcome [Fig. 2(d)] shows a broadened spectral distribution and undesired frequency correlation between the two photons. The output is a superposition of the directly transmitted state and the two-photon bound state [54–56], which corresponds to the first term and the second term in Eq. (2). Therefore, the CZ gate is not obtained because the artificial atom not only induces a  $\pi$  phase change but also induces the entanglement of other degrees of freedom. Such a problem was also predicted in a previous Kerr-type nonlinear medium [41,42], and the reason is attributed to the continuum modes in the waveguide: the excitation states  $|01\rangle$  and  $|20\rangle$  of the artificial atom could spontaneously emit photon pairs without conserving the frequency of individual photons, although the total energy  $p_1 + p_2$  of the two photons is conserved.

The direct two-photon interaction mediated by the artificial atom prevents the building of a quantum logic gate. In other words, the two-photon spontaneous-emission channels of the artificial atom must be suppressed during the gate operation, and thus the coupling between the continuum and the two-photon energy levels of the artificial atom should be shut off. Therefore, we introduce a scheme based on storing the control photon in the artificial atom to avoid the decay of the control photon to the continuum during its interaction with the target photon, and realize a photon-photon quantum phase gate on the PIC.

#### B. Photonic molecule scheme

As shown in Fig. 3(a), an architecture based on the photonic molecule is proposed to induce the  $\chi^{(2)}$  interaction in Fig. 2(b) and perform the CZ gate. The architecture is composed of two microresonators and a bus waveguide, with one microresonator engineered for the artificial atom and the other serving as an antenna to simultaneously couple with the artificial atom and waveguide. Since the two microresonators are made of the same  $\chi^{(2)}$  material, the frequency of the antenna can be modulated by the EO effect and thereby the coupling between the waveguide and artificial atom can be controlled in real time. Such a photonic molecule can be experimentally realized in LN integrated microrings and has been demonstrated to store coherent lasers [31]. The Hamiltonian of the system reads

$$H = H_{AA} + \omega_d d^\dagger d + \sum_{A \in \{a,b\}} [\Omega_A(t) A d^\dagger + \text{h.c.}], \quad (6)$$

where  $d$  is the bosonic operator for the ancillary mode (frequency  $\omega_d$ ) in the antenna cavity and  $A \in \{a, b\}$  is the operator for the modes in the artificial atom. By careful

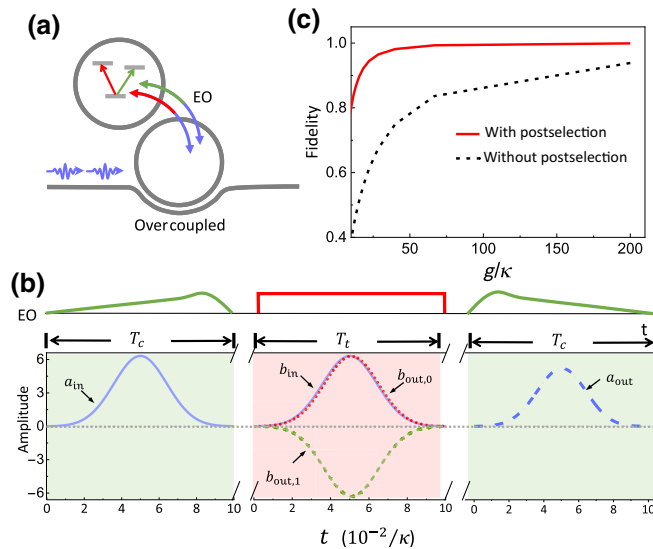


FIG. 3. The photon-photon controlled-phase gate in a photonic molecule. (a) Schematic of a photonic molecule. The cavity coupled to the waveguide serves as an active antenna as shown in Fig. 2(b). (b) Time sequence of the EO drive for the quantum storage and retrieval of the photons. In the calculation,  $\kappa_{d,1} = 10^3 \kappa_{d,0}$ ,  $\kappa_{d,0} = 2\kappa$ , and the intrinsic decay rate of the artificial atom  $\kappa_{a,0} = \kappa_{b,0} = \kappa = 1$ . The pulse shape of the control photon is a Gaussian function  $a_{in}^c = \alpha \{ \exp[-25(t/T_c - 0.5) - \exp(-6.25)] \}$ , and similarly for the target photon  $b_{in}^t$ .  $\alpha$  is the normalization factor. The duration of the two photons is  $T_c = T_t = 0.1/\kappa$ . (c) Gate fidelity versus nonlinear coupling strength  $g$ .

design of the geometry and tuning of the microresonators, the two cavities have slightly different free spectral ranges. The mode  $d$  is detuned from both mode  $a$  and mode  $b$ , and the coupling  $\Omega_{a,b}(t)$  between  $d$  and  $a$  or  $b$  can be switched by controlling the EO driving. For a strongly overcoupled antenna cavity with external coupling rate  $\kappa_{d,1} \gg \kappa_{d,0}$  ( $\kappa_{d,0}$  is the intrinsic loss rate of the antenna cavity), it can be adiabatically eliminated and this mediates the effective coupling between the waveguide and the artificial atom. For the input field  $A_{in}(t)$  for  $A \in \{a, b\}$ , the dynamics of the mode  $A$  of the artificial atom follows [57]

$$\frac{d}{dt}A = -i[A, H_{AA}] - (\tilde{\kappa}_{A,0} + \tilde{\kappa}_{A,1})A + \sqrt{2\tilde{\kappa}_{A,1}}A_{in}(t), \quad (7)$$

with  $\tilde{\kappa}_{A,0} \approx \kappa_{A,0} + |\Omega_A(t)|^2 \kappa_{d,0} / (\kappa_{d,0} + \kappa_{d,1})^2$  and  $\tilde{\kappa}_{A,1} \approx |\Omega_A(t)|^2 \kappa_{d,1} / (\kappa_{d,0} + \kappa_{d,1})^2$  denoting the time-dependent effective external coupling rate controlled by the antenna. By optimization of the shape and frequency of the EO field  $\Omega_A(t)$ , the antenna can couple photons of different shapes and frequencies in the waveguide to different energy levels. To avoid crosstalk during the operation, the nondegenerate

$\chi^{(2)}$  interaction is used and the EO drives have different frequencies.

Figure 3(b) shows the sequence of the CZ-gate scheme. Initially, quantum states are encoded in control ( $|\psi_c\rangle = \alpha_c|0\rangle_c + \beta_c|1\rangle_c$ ) and target ( $|\psi_t\rangle = \alpha_t|0\rangle_t + \beta_t|1\rangle_t$ ) photons, which are temporally separated and sent to the photonic molecule. These two photons can be coupled to the artificial atom only if they are prepared in state  $|1\rangle$ , which can be realized by the dual-rail encoding shown in Fig. 2(b). Under an appropriate EO drive, the control photon of shape  $a_{in}(t)$  is stored in the artificial atom ( $|\psi_{AA}\rangle = \alpha_c|000\rangle + \beta_c|100\rangle$ ). Subsequently, the target photon of shape  $b_{in}(t)$  comes and another EO drive with strength  $\kappa_{b,0} \ll \Omega_b \ll g$  is applied. Because of the strong  $\chi^{(2)}$  interaction, the transition  $|100\rangle \rightarrow |110\rangle$  is blocked, while the transition  $|000\rangle \rightarrow |010\rangle$  is allowed. Thus, the target photon will be reflected back to the waveguide and acquires a  $\pi$  phase depending on the state of the artificial atom. The state becomes  $\alpha_c|000\rangle \otimes |\psi_t\rangle + \beta_c|100\rangle \otimes Z|\psi_t\rangle$ , manifesting the CZ gate, where  $Z$  denotes the Pauli matrix. Finally, another EO drive is applied to retrieve the control photon to the waveguide. During the whole process, the two photons never meet each other and two-photon spontaneous emission is avoided.

### C. Control-photon storage and retrieval

To ensure high fidelity, not only the pulse shapes of the photons are required to be preserved but also the storage and retrieval efficiency should be as high as possible. Since the two photons are operated independently, the storage and retrieval are the time-reverse of each other. The single-photon state is expressed as  $|\psi\rangle_{da} = c_{10}|10\rangle + c_{01}|01\rangle$ , where  $|mn\rangle = |m\rangle_d \otimes |n\rangle_a$  denotes the Fock states, with  $d$  being the antenna cavity mode. Under single-photon pulse excitation of a perfectly-phase-matched cavity, the dynamics of the intracavity and output fields follow

$$\frac{d}{dt}c_{10} = -\kappa_d c_{10} - i\Omega^*(t)c_{01} + \sqrt{2\kappa_{d,1}}A_{in}(t), \quad (8)$$

$$\frac{d}{dt}c_{01} = -\kappa_d c_{01} - i\Omega(t)c_{10}, \quad (9)$$

$$A_{out} = A_{in} - \sqrt{2\kappa_{d,1}}c_{10}, \quad (10)$$

where  $A_{in}(t)$  [ $A_{out}(t)$ ] represents the pulse shape of the input (output) single photon. The goal is to store the input control photon as  $|01\rangle$  and retrieve it from the cavity after the gate operation. For the storage process, we assume that both cavities are initially in the ground state ( $c_{10} = c_{01} = 0$ ), and also assume that the input field excitation  $A_{in}(t)$  has nonzero values only in time interval  $[0, T]$ , where  $\int_0^T dt |A_{in}(t)|^2 = 1$ . Then the storage efficiency is given by

$$\eta_s = |c_{01}(T)|^2. \quad (11)$$

For the retrieval process, we set  $c_{10}(t_r) = 0$ ,  $c_{01}(t_r) = 1$ , with  $t_r$  being the start time of the retrieval. Then, the retrieval efficiency is given by

$$\eta_r = \int_{t_r}^{\infty} |A_{\text{out}}(t)|^2 dt. \quad (12)$$

During the retrieval process with  $A_{\text{in}}(t) = 0$  for  $t > t_r$ , we have

$$\frac{d}{dt} (|c_{10}|^2 + |c_{01}|^2) = -2\kappa_d |c_{10}|^2 \quad (13)$$

in the situation where the quality factor of the artificial atom is much larger than that of the ancillary mode, since the latter overcouples with a bus waveguide. Therefore, the retrieval efficiency is derived as

$$\begin{aligned} \eta_r &= 2\kappa_{d,1} \int_{t_r}^{\infty} dt |c_{10}|^2 \\ &= \frac{\kappa_{d,1}}{\kappa_{d,0} + \kappa_{d,1}} \\ &\times (|c_{10}(t_r)|^2 + |c_{01}(t_r)|^2 - |c_{10}(\infty)|^2 - |c_{01}(\infty)|^2). \end{aligned}$$

If there is no excitation in the cavity after the retrieval process,  $|c_{10}(\infty)|^2 = |c_{01}(\infty)|^2 = 0$ , the efficiency reduces to

$$\eta_r = \frac{\kappa_{d,1}}{\kappa_{d,0} + \kappa_{d,1}}. \quad (14)$$

This expression indicates the retrieval efficiency is independent of the pulse shape of the driving fields, provided that the driving field pumps all excitation out of the cavity completely. To achieve high retrieval efficiency, an overcoupled condition of the waveguide-ancillary cavity system is required.

The driving field for the retrieval process can be derived under the adiabatic approximation with  $\kappa_d \gg g/T$ , which gives a smooth pulse shape, and also adiabatic elimination of the population of state  $|10\rangle$ ; that is, Eq. (8) reduces to  $-\kappa_d c_{10} - i\Omega c_{01} = 0$ . If we substitute this into Eq. (9), we get

$$\frac{d}{dt} c_{01} = -\frac{|\Omega(t)|^2}{\kappa_d} c_{01} \quad (15)$$

and thus obtain

$$c_{01}(t) = e^{-(1/\kappa_d) \int_0^t |\Omega(t')|^2 dt'} \quad (16)$$

using the boundary condition  $c_{01}(0) = 1$  (the start time of the retrieval process is set to be 0 for simplicity). If we

denote  $\Theta(t, t') = \int_t^{t'} |\Omega(t'')|^2 dt''$ , the output field is derived by Eq. (10) as

$$A_{\text{out}}(t) = i \frac{\sqrt{2\kappa_{d,1}}}{\kappa_d} \Omega(t) e^{-(1/\kappa_d)\Theta(0,t)}. \quad (17)$$

We compute the retrieval efficiency using Eq. (17):

$$\begin{aligned} \eta_r &= \int_0^{\infty} dt |A_{\text{out}}(t)|^2 \\ &= \frac{\kappa_{d,1}}{\kappa_{d,0} + \kappa_{d,1}} (1 - e^{-(2/\kappa_d)\Theta(0,\infty)}). \end{aligned}$$

For a strong or long driving pulse,  $\Theta(0, \infty) \gg 1$ , the retrieval efficiency reduces to the previously derived form [Eq. (14)].

To be more practical, we consider the case that not all excitations are driven out of the cavity, which means either  $c_{01}(\infty)$  or  $c_{10}(\infty)$  does not equal zero. The efficiency can be obtained by giving  $\Theta(0, \infty)$  a finite value. Here we shape the driving field  $\Omega(t)$  to retrieve the photon to the desired mode  $A_{\text{in}}(t)$  (the input shape). Equaling  $\sqrt{\kappa_{d,1}/(\kappa_{d,0} + \kappa_{d,1})} A_{\text{in}}(t)$  and Eq. (17) and their norm square integrals, we obtain

$$\int_0^t dt' |A_{\text{in}}(t')|^2 = 1 - e^{-(2/\kappa_d)\Theta(0,t)}. \quad (18)$$

We derive the optimal retrieval pulse shape:

$$\begin{aligned} \Omega(t) &= -i \sqrt{\frac{\kappa_d}{2}} e^{\Theta(0,t)/\kappa_c} A_{\text{in}}(t) \\ &= -i \sqrt{\frac{\kappa_d}{2}} \frac{A_{\text{in}}(t)}{\sqrt{\int_t^{\infty} dt' |A_{\text{in}}(t')|^2}}. \end{aligned} \quad (19)$$

The optimal drive for the storage process is the time-reverse of that for the retrieval process, and one can use the driving pulse  $\Omega^*(t_r - t)$  to store the input pulse of shape  $A_{\text{in}}(t)$  with maximal efficiency. It is shown that the quantum storage and retrieval efficiencies are independent of the pulse shape [58], and efficiency higher than 99.9% is expected for the strongly overcoupled antenna due to the very large coupling rate  $\kappa_{d,1}/\kappa_{d,0} > 10^3$  between the waveguide and the cavity.

## D. Transmission of target photon

For the operations on both the control photon and the target photon, there are at most two excitations, and thus the quantum dynamics of the system [Eq. (7)] can be solved in a truncated Fock-state space. Since the nonlinear interaction happens when the control photon is already stored in the cavity, we calculate only the transmission of the target photon encoded in state  $|1\rangle_t$ . The quantum state of

the target photon  $|1\rangle_t$  can be expressed in the time domain as  $|\psi\rangle = \int dt A_{\text{in}}(t) b^\dagger(t) |\emptyset\rangle$ . The normalization condition requires  $\int_0^T dt |A_{\text{in}}(t)|^2 = 1$  for the input state.

In the two-excitation subspace, the state can be described by a pure state with a general form of the superposition of Fock states. For one control photon initially stored in mode  $a$  with a long lifetime, the state of the system can be expressed as

$$|\psi\rangle_{dbac} = c_{1010}|1010\rangle + c_{0110}|0110\rangle + c_{0001}|0001\rangle, \quad (20)$$

where  $|mnkl\rangle$  denotes Fock state  $m, n, k, l$  in modes  $d, b, a$ , and  $c$ , respectively. Here  $d$  is the ancillary cavity mode,  $a$  is the mode that stores the control photon,  $b$  is the mode that matches the target photon, and  $c$  is the second-harmonic mode. According to the system Hamiltonian, the dynamics follows

$$\frac{d}{dt}c_{1010} = -\kappa_d c_{1010} - \kappa_a c_{1010} - i\Omega c_{0110} - iA_{\text{in}}(t), \quad (21)$$

$$\frac{d}{dt}c_{0110} = -\kappa_b c_{0110} - \kappa_a c_{0110} - i\Omega c_{1010} - ig_{\text{nd}} c_{0001}, \quad (22)$$

$$\frac{d}{dt}c_{0001} = -\kappa_c c_{0001} - ig_{\text{nd}} c_{0110}. \quad (23)$$

We set the initial state as  $c_{1010} = c_{0110} = c_{0001} = 0$  to solve the dynamics of the system. For EO driving strength  $\kappa_A \ll \Omega \ll g_{\text{nd}}$ , the waveguide is effectively overcoupled with the atom. The target photon couples into and out of the atom for the control photon in state  $|0\rangle_c$ , whereas it transmits directly without entering the atom for the control photon in state  $|1\rangle_t$ . In this case, it is no longer necessary to design the shape of the EO drive, but an appropriate strength should be carefully chosen. For a cavity quality factor of  $10^7$ , corresponding to a decay rate of about 10 MHz,  $\Omega$  is required to be 1–10 GHz, which can be realized with EO modulators under the current experimental conditions.

For Fig. 3(b), we calculate the evolution of the pulse shape for both photons. It is shown that the shapes of the output fields  $b_{\text{out},0}$  and  $b_{\text{out},1}$  (subscripts 0 and 1 denote the output conditioned on control state  $|0\rangle_c$  or  $|1\rangle_t$ ) for the target photon and  $a_{\text{out}}$  for the control photon are nearly the same as their inputs, indicating the high fidelity of the quantum gate. The  $\pi$  phase shift is indicated by the negativity of  $b_{\text{out},1}$ . The relationship between the gate fidelity and  $g/\kappa$  (the atom decay rate  $\kappa_{A,0} = \kappa$ ) is plotted in Fig. 3(c) (dashed line). The gate fidelity is defined as the state fidelity between the real output state and the ideal output state with input state of  $|\psi\rangle = \frac{1}{\sqrt{2}}(|0\rangle_c + |1\rangle_c) \otimes \frac{1}{\sqrt{2}}(|0\rangle_t + |1\rangle_t)$ . In our case, the main imperfection affecting the gate fidelity is the lifetime of the atomic states, which decays during the transmission of the target photon. By normalization of the output state via postselection

of the two-photon events, the gate fidelity can be as high as 99% for  $g/\kappa \sim 100$  [Fig. 3(c), solid line].

Recalling that the internal states of an artificial atom can be manipulated through coherent driving [Fig. 1(c)], the artificial atom can also be used to mediate the entanglement between photons. For example, the Duan-Kimble protocol [59] and the Lindner-Rudolph protocol [60] can be realized without photon storage and retrieval, but require the manipulation of the internal state of the artificial atom. These protocols are feasible in light of the fact that two-photon spontaneous emission is avoided. Additionally, the higher-excitation eigenstates of the artificial atom can also be engineered to construct quantum gates for the multilevel encoding of quantum states.

#### IV. DISCUSSION AND CONCLUSION

From these studies, the performances of artificial atoms depend on  $g/\kappa$ , as a benchmark for the cooperation of nonlinear optical processes at the single-photon-level. Among various available platforms, LN is appealing. It has a high  $\chi^{(2)}$  susceptibility of about  $4 \times 10^{-11}$  m/V and excellent electro-optic behavior. Recent advances in its etching have resulted in the quality factor of an integrated LN microcavity with a diameter of tens of micrometers of up to approximately  $10^7$  for phase-matched nonlinear frequency conversion [28], corresponding to an intrinsic cavity decay rate ( $\kappa_0$ ) of 10 MHz. More excitingly, the intrinsic quality factor of the LN microcavity limited by material absorption is higher than  $10^9$  [31], implying  $\kappa_0 \sim 0.1$  MHz. With a periodically poled LN-microring resonator for better phase matching, Lu *et al.* demonstrated the second-order nonlinear coupling strength to be 1.58 MHz with effective  $\chi^{(2)}$  3.63 pm/V in experiments. By use of the  $d_{33}$  nonlinear susceptibility, the nonlinear coupling strength can be increased to about 17 MHz with a cavity of similar size and quality factor. More recently, Zhang *et al.* [61] reported a LN microcavity with a quality factor as high as  $4.7 \times 10^7$ . Therefore, with optimized phase-matching conditions, a  $g/\kappa$  of about 10 is achievable with current fabrication technology. By further reduction of the photonic mode volume below  $200 \mu\text{m}^3$  and increase of the cavity factor to  $5 \times 10^8$ ,  $g/\kappa$  could reach 100.

There are also many other potential candidates for artificial atoms. Other materials with excellent nonlinear-optics properties, such as GaAs [27], organic single crystals [62], and two-dimensional materials [63], have been developed recently and are compatible with current PIC platforms [64]. At the same time, new techniques to engineer  $\chi^{(2)}$  nonlinearity have been developed [65]. For example, an effective  $\chi^{(2)}$  effect can be induced in centrosymmetric materials, such as silicon waveguides, by applying an external-bias electric field [66].

In conclusion, we introduce an artificial atom on a photonic integrated circuit by harnessing the cavity-enhanced

optical  $\chi^{(2)}$  nonlinearity. Such an artificial atom preserves the advantages of both the atom and the photonic cavity, and offers single-photon-level nonlinearity for deterministic quantum gates as well as experimental compatibility and flexibility for scalable quantum devices. Moreover, we propose a scheme based on the artificial atom to realize a high-fidelity two-photonic-qubit quantum controlled-phase gate by switching the coupling channels between the artificial atom and the continuum, which also addresses the concerns raised by Shapiro *et al.* [37,39]. Because of recent advances in the development of low-loss thin-film LN on an insulator platform, an artificial atom with  $g/\kappa \sim 1$  is currently feasible, and thereby quantum effects (such as photon blockade) could be envisioned in a photonic chip made with pure dielectrics. The universal-quantum-gate set [47] would also be achievable, paving the way toward room-temperature, single-emitter-free quantum-information processing.

## ACKNOWLEDGMENTS

This work was funded by the National Key R & D Program (Grant No. 2016YFA0301300), the National Natural Science Foundation of China (Grants No. 11874342, No. 11934012, No. 11922411, No. 11904316, and No. 11704370), the Anhui Initiative in Quantum Information Technologies (Grant No. AHY130200), and the China Postdoctoral Science Foundation (Grant No. 2019M662153).

*Note added.*—While we were finalizing the manuscript, a related theoretical study was posted on arXiv [67].

## APPENDIX

Here we derive the two-photon transportation through a waveguide side coupled to a cavity supporting  $\chi^{(2)}$  interaction. The waveguide supports continuum states in the fundamental ( $f$ ) and second-harmonic ( $s$ ) frequency bands. Inside the cavity, modes  $a$  and  $c$  couple with each other via the process of second-harmonic generation. The Hamiltonian of the whole system includes the continuum states in the waveguide

$$H_W = \int dx \left[ f^\dagger(x) \frac{1}{i} \frac{d}{dx} f(x) + s^\dagger(x) \frac{1}{i} \frac{d}{dx} s(x) \right], \quad (\text{A1})$$

the localized states in the cavity

$$H_C = (\omega_a - i\kappa_{a,0}) a^\dagger a + (\omega_c - i\kappa_{c,0}) c^\dagger c, \quad (\text{A2})$$

the nonlinear coupling inside the cavity

$$H_{nl} = g_d (a^{\dagger 2} c + a^2 c^\dagger), \quad (\text{A3})$$

and the linear coupling between the waveguide and cavity

$$H_l = V_a \int dx \delta(x) [f^\dagger(x) a + f(x) a^\dagger] + V_c \int dx \delta(x) [s^\dagger(x) c + s(x) c^\dagger], \quad (\text{A4})$$

where  $x$  is coordinate along the waveguide,  $f(x)$  [ $s(x)$ ] and  $f^\dagger(x)$  [ $s^\dagger(x)$ ] are the annihilation and creation operators at position  $x$  in the waveguide,  $g_d$  is the nonlinear coupling strength of SHG,  $V_a$  ( $V_c$ ) is the coupling strength between the waveguide and the cavity in the fundamental (second-harmonic) frequency band, and  $\kappa_{a,0}$  ( $\kappa_{c,0}$ ) is the intrinsic decay rate of the cavity mode. Since the coupling near the narrow resonant-frequency window is considered, the dispersions of the coupling strengths  $g_d$ ,  $V_a$ , and  $V_c$  are ignored. The input state is initially prepared in a two-photon state at the fundamental frequencies. A general form of the two-excitation state can be written as

$$\begin{aligned} |E_2\rangle = & \int dx_1 dx_2 g(x_1, x_2) f^\dagger(x_1) f^\dagger(x_2) |\emptyset\rangle \\ & + \int dx m(x) f^\dagger(x) a^\dagger |\emptyset\rangle + \int dx h(x) s^\dagger(x) |\emptyset\rangle \\ & + f_a \frac{1}{\sqrt{2}} a^\dagger a^\dagger |0\rangle + f_c c^\dagger |\emptyset\rangle, \end{aligned} \quad (\text{A5})$$

with  $|\emptyset\rangle$  being the vacuum state. Following the Schrödinger equation  $H|E_2\rangle = E_2|E_2\rangle$  ( $E_2 = k_1 + k_2$ ,  $k_i$  is the frequency of the  $i$ th photon), one gets

$$\begin{aligned} & \left( -i \frac{\partial}{\partial x_1} - i \frac{\partial}{\partial x_2} - E_2 \right) g(x_1, x_2) \\ & + \frac{V_a}{2} [\delta(x_1)m(x_2) + \delta(x_2)m(x_1)] = 0, \end{aligned} \quad (\text{A6})$$

$$\begin{aligned} & \left( -i \frac{d}{dx} + \omega_a - i\kappa_{a,0} - E_2 \right) m(x) \\ & + V_a [g(x, 0) + g(0, x)] + \sqrt{2} V_a f_a \delta(x) = 0, \end{aligned} \quad (\text{A7})$$

$$\left( -i \frac{d}{dx} - E_2 \right) h(x) + V_c f_c \delta(x) = 0, \quad (\text{A8})$$

$$(2\omega_a - 2i\kappa_{a,0} - E_2) f_a + \sqrt{2} g_d f_c + \sqrt{2} V_a m(0) = 0, \quad (\text{A9})$$

$$(\omega_c - i\kappa_{c,0} - E_2) f_c + \sqrt{2} g_d f_a + V_c h(0) = 0. \quad (\text{A10})$$

Using the discontinuous functions

$$g(x, 0) = g(0, x), \quad (\text{A11})$$

$$g(x, 0) = [g(x, 0^+) + g(x, 0^-)]/2, \quad (\text{A12})$$

$$m(0) = [m(0^+) + m(0^-)]/2, \quad (\text{A13})$$

$$h(0) = [h(0^+) + h(0^-)]/2, \quad (\text{A14})$$

$$\frac{d}{dx} m(x) \Big|_{x=0} = [m(0^+) - m(0^-)]\delta(x), \quad (\text{A15})$$

we get

$$\begin{aligned} & \left( -i \frac{d}{dx} + \omega_a - i\kappa_{a,0} - i\kappa_{a,1} - E_2 \right) g(0^+, x) \\ &= \left( -i \frac{d}{dx} + \omega_a - i\kappa_{a,0} + i\kappa_{a,1} - E_2 \right) g(0^-, x). \end{aligned} \quad (\text{A16})$$

With use of the method in Ref. [52],  $g(x_1, x_2)$  is divided to three regions:  $g_1(x_1, x_2)$  for  $x_1 \leq x_2 < 0$ ,  $g_2(x_1, x_2)$  for  $x_1 < 0 < x_2$ , and  $g_3(x_1, x_2)$  for  $0 < x_1 \leq x_2$ . For the two-photon monochromatic wave input state

$$g_1(x_1, x_2) = \frac{1}{2\sqrt{2}\pi} (e^{ik_1 x_1} e^{ik_2 x_2} + e^{ik_2 x_1} e^{ik_1 x_2}),$$

$g(x_1, x_2)$  in the other two regions is derived from Eq. (A16) as

$$\begin{aligned} g_2(x_1, x_2) &= \frac{1}{2\sqrt{2}\pi} (t_{k_2} e^{i(k_1 x_1 + k_2 x_2)} + t_{k_1} e^{i(k_2 x_1 + k_1 x_2)}), \\ g_3(x_1, x_2) &= \frac{1}{2\sqrt{2}\pi} t_{k_1} t_{k_2} (e^{i(k_1 x_1 + k_2 x_2)} + e^{i(k_2 x_1 + k_1 x_2)}) \\ &\quad + B e^{-i(\omega_a - i\kappa_{a,0} - i\kappa_{a,1})(x_2 - x_1)} e^{i(k_1 + k_2)x_2}, \end{aligned}$$

with

$$t_k = \frac{k - \omega_a + i\kappa_{a,0} - i\kappa_{a,1}}{k - \omega_a + i\kappa_{a,0} + i\kappa_{a,1}}. \quad (\text{A17})$$

Eliminating  $f_a$  and  $f_c$ , we obtain

$$\begin{aligned} & \frac{2i}{V_a} [\xi_a^- g(0^+, 0^+) - (\xi_a^- + \xi_a^+) g(0^-, 0^+) + \xi_a^+ g(0^-, 0^-)] \\ &+ 2g_d \frac{V_a}{V_c} [h(0^+) - h(0^-)] = 0, \\ & \xi_b^- h(0^+) - \xi_b^+ h(0^-) \\ &+ \frac{2ig_d V_c}{V_a^2} [g(0^+, 0^+) - 2g(0^-, 0^+) + g(0^-, 0^-)] = 0, \end{aligned}$$

with  $\xi_a^\pm = 2(\omega_a - i\kappa_{a,0} \pm i\kappa_{a,1}) - k_1 - k_2$  and  $\xi_c^\pm = (\omega_c - i\kappa_{c,0} \pm i\kappa_{c,1}) - k_1 - k_2$ , where  $\kappa_{i,1} = V_i^2/2$ . Using the values at the discontinuous conditions, one finally obtains

$$\begin{aligned} C &= -\frac{2g_d \sqrt{2\kappa_{c,1}} (2 - t_{k_1} - t_{k_2})}{\sqrt{\pi} (\xi_a^- \xi_c^- - 2g_d^2)}, \\ B &= \frac{\sqrt{2}g_d^2 (1 - t_{k_1}) (1 - t_{k_2})}{\pi (\xi_a^- \xi_c^- - 2g_d^2)}. \end{aligned}$$

The wave functions of the two-photon input and output states are computed as

$$\begin{aligned} \phi_{\text{in}}(x_1, x_2) &= g_1(x_1, x_2)\theta(x_2 - x_1) + g_1(x_2, x_1)\theta(x_1 - x_2), \\ \phi_{\text{out}}(x_1, x_2) &= g_3(x_1, x_2)\theta(x_2 - x_1) + g_3(x_2, x_1)\theta(x_1 - x_2), \end{aligned}$$

where  $\theta(x)$  is the step function. Then the two-photon scattering matrix is obtained by calculating the wave-function overlap between the output state and the two-photon plane-wave state:

$$\begin{aligned} S(p_1, p_2; k_1, k_2) &= \int dx_1 dx_2 \frac{1}{2\sqrt{2}\pi} (e^{-i(p_1 x_1 + p_2 x_2)} + e^{-i(p_2 x_1 + p_1 x_2)}) \\ &\times \phi_{\text{out}}(x_1, x_2). \end{aligned}$$

The transmission plane-wave term is

$$S_{\text{plane}} = S_{p_1 k_1} S_{p_2 k_2} + S_{p_1 k_2} S_{p_2 k_1},$$

where  $S_{pk} = t_k \delta(p - k)$ . The bound-state term is

$$S_{\text{bound}} = \frac{B}{\sqrt{2\kappa_{a,1}}} (2 - t_{p_1} - t_{p_2}) \delta(p_1 + p_2 - k_1 - k_2).$$

The total scattering matrix is

$$\begin{aligned} S(p_1, p_2; k_1, k_2) &= t_{k_1} t_{k_2} [\delta(p_1 - k_1) \delta(p_2 - k_2) + \delta(p_1 - k_2) \delta(p_2 - k_1)] \\ &+ \frac{B}{\sqrt{2\kappa_{a,1}}} (2 - t_{p_1} - t_{p_2}) \delta(p_1 + p_2 - k_1 - k_2). \end{aligned} \quad (\text{A18})$$

According to the scattering matrix, one can compute the output spectrum of the two-photon state as

$$\phi_{\text{out}}(p_1, p_2) = \iint \phi_{\text{in}}(k_1, k_2) S(p_1, p_2; k_1, k_2) dk_1 dk_2, \quad (\text{A19})$$

where  $\phi_{\text{in}}(k_1, k_2)$  is the input spectrum.

- [1] A. Politi, J. C. F. Matthews, M. G. Thompson, and J. L. O'Brien, Integrated quantum photonics, *IEEE J. Sel. Top. Quantum Electron.* **15**, 1673 (2009).
- [2] S. Takeda and A. Furusawa, Toward large-scale fault-tolerant universal photonic quantum computing, *APL Photonics* **4**, 060902 (2019).
- [3] T. D. Ladd, F. Jelezko, R. Laflamme, Y. Nakamura, C. Monroe, and J. L. O'Brien, Quantum computers, *Nature* **464**, 45 (2010).
- [4] A. Aspuru-Guzik and P. Walther, Photonic quantum simulators, *Nat. Phys.* **8**, 285 (2012).
- [5] A. Politi, J. C. F. Matthews, and J. L. O'Brien, Shor's quantum factoring algorithm on a photonic chip, *Science* **325**, 1221 (2009).
- [6] L. Caspani, C. Xiong, B. J. Eggleton, D. Bajoni, M. Liscidini, M. Galli, R. Morandotti, and D. J. Moss, Integrated sources of photon quantum states based on nonlinear optics, *Light: Sci. Appl.* **6**, e17100 (2017).
- [7] A. Politi, M. J. Cryan, J. G. Rarity, S. Yu, and J. L. O'Brien, Silica-on-silicon waveguide quantum circuits, *Science* **320**, 646 (2008).
- [8] A. Crespi, R. Ramponi, R. Osellame, L. Sansoni, I. Bonfigiani, F. Sciarrino, G. Vallone, and P. Mataloni, Integrated photonic quantum gates for polarization qubits, *Nat. Commun.* **2**, 566 (2011).
- [9] F. Najafi, J. Mower, N. C. Harris, F. Bellei, A. Dane, C. Lee, X. Hu, P. Kharel, F. Marsili, S. Assefa, K. K. Berggren, and D. Englund, On-chip detection of non-classical light by scalable integration of single-photon detectors, *Nat. Commun.* **6**, 5873 (2015).
- [10] R. Cheng, X. Guo, X. Ma, L. Fan, K. Y. Fong, M. Poot, and H. X. Tang, Self-aligned multi-channel superconducting nanowire single-photon detectors, *Opt. Express* **24**, 27070 (2016).
- [11] J. P. Sprengers, A. Gaggero, D. Sahin, S. Jahanmirinejad, G. Frucci, F. Mattioli, R. Leoni, J. Beetz, M. Lermer, M. Kamp, S. Höfling, R. Sanjines, and A. Fiore, Waveguide superconducting single-photon detectors for integrated quantum photonic circuits, *Appl. Phys. Lett.* **99**, 181110 (2019).
- [12] S. Khasminskaya, F. Pyatkov, K. Słowik, S. Ferrari, O. Kahl, V. Kovalyuk, P. Rath, A. Vetter, F. Hennrich, M. M. Kappes, G. Gol'tsman, A. Korneev, C. Rockstuhl, R. Krupke, and W. H. P. Pernice, Fully integrated quantum photonic circuit with an electrically driven light source, *Nat. Photonics* **10**, 727 (2016).
- [13] R. W. Boyd, *Nonlinear Optics* (Academic press, New York, 2003).
- [14] J. L. O'Brien, A. Furusawa, and J. Vučković, Photonic quantum technologies, *Nat. Photonics* **3**, 687 (2009).
- [15] A. V. Gorshkov, J. Otterbach, M. Fleischhauer, T. Pohl, and M. D. Lukin, Photon-Photon Interactions via Rydberg Blockade, *Phys. Rev. Lett.* **107**, 133602 (2011).
- [16] T. G. Tiecke, J. D. Thompson, N. P. de Leon, L. R. Liu, V. Vuletić, and M. D. Lukin, Nanophotonic quantum phase switch with a single atom, *Nature* **508**, 241 (2014).
- [17] B. Hacker, S. Welte, G. Rempe, and S. Ritter, A photon-photon quantum gate based on a single atom in an optical resonator, *Nature* **536**, 193 (2016).
- [18] K. J. Vahala, Optical microcavities, *Nature* **424**, 839 (2003).
- [19] D. V. Strekalov, C. Marquardt, A. B. Matsko, H. G. Schweißfel, and G. Leuchs, Nonlinear and quantum optics with whispering gallery resonators, *J. Opt.* **18**, 123002 (2016).
- [20] G. Lin, A. Coillet, and Y. K. Chembo, Nonlinear photonics with high-q whispering-gallery-mode resonators, *Adv. Opt. Photon.* **9**, 828 (2017).
- [21] A. W. Bruch, X. Liu, J. B. Surya, C.-L. Zou, and H. X. Tang, On-chip  $\chi^{(2)}$  microring optical parametric oscillator, *Optica* **6**, 1361 (2019).
- [22] Q. Li, M. Davanço, and K. Srinivasan, Efficient and low-noise single-photon-level frequency conversion interfaces using silicon nanophotonics, *Nat. Photonics* **10**, 406 (2016).
- [23] X. Guo, C. L. Zou, H. Jung, and H. X. Tang, On-Chip Strong Coupling and Efficient Frequency Conversion between Telecom and Visible Optical Modes, *Phys. Rev. Lett.* **117**, 123902 (2016).
- [24] T. J. Kippenberg, A. L. Gaeta, M. Lipson, and M. L. Gorodetsky, Dissipative kerr solitons in optical microresonators, *Science* **361**, eaan8083 (2018).
- [25] M. Li, C.-L. Zou, C.-H. Dong, and D.-X. Dai, Optimal third-harmonic generation in an optical microcavity with  $\chi^{(2)}$  and  $\chi^{(3)}$  nonlinearities, *Opt. Express* **26**, 27294 (2018).
- [26] A. W. Bruch, X. Liu, X. Guo, J. B. Surya, Z. Gong, L. Zhang, J. Wang, J. Yan, and H. X. Tang, 17 000%/w second-harmonic conversion efficiency in single-crystalline aluminum nitride microresonators, *Appl. Phys. Lett.* **113**, 131102 (2019).
- [27] L. Chang, A. Boes, P. Pintus, J. D. Peters, M. Kennedy, X.-W. Guo, N. Volet, S.-P. Yu, S. B. Papp, and J. E. Bowers, Strong frequency conversion in heterogeneously integrated gaas resonators, *APL Photonics* **4**, 036103 (2019).
- [28] J. Lin, N. Yao, Z. Hao, J. Zhang, W. Mao, M. Wang, W. Chu, R. Wu, Z. Fang, L. Qiao, W. Fang, F. Bo, and Y. Cheng, Broadband Quasi-Phase-Matched Harmonic Generation in an On-Chip Monocrystalline Lithium Niobate Microdisk Resonator, *Phys. Rev. Lett.* **122**, 173903 (2019).
- [29] J. Lu, J. B. Surya, X. Liu, A. W. Bruch, Z. Gong, Y. Xu, and H. X. Tang, Periodically poled thin-film lithium niobate microring resonators with a second-harmonic generation efficiency of 250,000%/w, *Optica* **6**, 1455 (2019).
- [30] M. Zhang, C. Wang, R. Cheng, A. Shams-Ansari, and M. Lončar, Monolithic ultra-high-q lithium niobate microring resonator, *Optica* **4**, 1536 (2017).
- [31] M. Zhang, C. Wang, Y. Hu, A. Shams-Ansari, T. Ren, S. Fan, and M. Lončar, Electronically programmable photonic molecule, *Nat. Photonics* **13**, 36 (2019).
- [32] J.-Y. Chen, Z.-H. Ma, Y. M. Sua, Z. Li, C. Tang, and Y.-P. Huang, Ultra-efficient frequency conversion in quasi-phase-matched lithium niobate microrings, *Optica* **6**, 1244 (2019).
- [33] X. Guo, C. Zou, and H. Tang, Second-harmonic generation in aluminum nitride microrings with 25000% W conversion efficiency, *Optica* **3**, 1126 (2016).
- [34] W. T. M. Irvine, K. Hennessy, and D. Bouwmeester, Strong Coupling between Single Photons in Semiconductor Microcavities, *Phys. Rev. Lett.* **96**, 057405 (2006).

- [35] S. Ferretti and D. Gerace, Single-photon nonlinear optics with kerr-type nanostructured materials, *Phys. Rev. B* **85**, 033303 (2012).
- [36] A. Majumdar and D. Gerace, Single-photon blockade in doubly resonant nanocavities with second-order nonlinearity, *Phys. Rev. B* **87**, 235319 (2013).
- [37] J. H. Shapiro, Single-photon kerr nonlinearities do not help quantum computation, *Phys. Rev. A* **73**, 062305 (2006).
- [38] J. Gea-Banacloche, Impossibility of large phase shifts via the giant kerr effect with single-photon wave packets, *Phys. Rev. A* **81**, 043823 (2010).
- [39] J. Dove, C. Chudzicki, and J. H. Shapiro, Phase-noise limitations on single-photon cross-phase modulation with differing group velocities, *Phys. Rev. A* **90**, 062314 (2014).
- [40] B. Fan, A. F. Kockum, J. Combes, G. Johansson, I.-C. Hoi, C. M. Wilson, P. Delsing, G. J. Milburn, and T. M. Stace, Breakdown of the Cross-Kerr Scheme for Photon Counting, *Phys. Rev. Lett.* **110**, 053601 (2013).
- [41] C. Chudzicki, I. L. Chuang, and J. H. Shapiro, Deterministic and cascadable conditional phase gate for photonic qubits, *Phys. Rev. A* **87**, 042325 (2013).
- [42] K. Xia, M. Johansson, P. L. Knight, and J. Twamley, Cavity-Free Scheme for Nondestructive Detection of a Single Optical Photon, *Phys. Rev. Lett.* **116**, 023601 (2016).
- [43] Y.-Z. Sun, Y.-P. Huang, and P. Kumar, Photonic Nonlinearities via Quantum Zeno Blockade, *Phys. Rev. Lett.* **110**, 223901 (2013).
- [44] J.-Y. Chen, Y. M. Sua, Z.-T. Zhao, M. Li, and Y.-P. Huang, Observation of quantum zeno blockade on chip, *Sci. Rep.* **7**, 14831 (2017).
- [45] S. R. Sathyamoorthy, L. Tornberg, A. F. Kockum, B. Q. Baragiola, J. Combes, C. M. Wilson, T. M. Stace, and G. Johansson, Quantum Nondemolition Detection of a Propagating Microwave Photon, *Phys. Rev. Lett.* **112**, 093601 (2014).
- [46] D. J. Brod and J. Combes, Passive Cphase Gate via Cross-Kerr Nonlinearities, *Phys. Rev. Lett.* **117**, 080502 (2016).
- [47] M. A. Nielsen and I. L. Chuang, *Quantum Computation and Quantum Information* (Cambridge University Press, Cambridge, 2010).
- [48] C. Hamsen, K. N. Tolazzi, T. Wilk, and G. Rempe, Two-Photon Blockade in an Atom-Driven Cavity QED System, *Phys. Rev. Lett.* **118**, 133604 (2017).
- [49] P. Krantz, M. Kjaergaard, F. Yan, T. P. Orlando, S. Gustavsson, and W. D. Oliver, A quantum engineer's guide to superconducting qubits, *Appl. Phys. Rev.* **6**, 021318 (2019).
- [50] J. R. Johansson, P. D. Nation, and F. Nori, Qutip 2: A python framework for the dynamics of open quantum systems, *Comput. Phys. Commun.* **184**, 1234 (2013).
- [51] P. Lodahl, S. Mahmoodian, S. Stobbe, A. Rauschenbeutel, P. Schneeweiss, J. Volz, H. Pichler, and P. Zoller, Chiral quantum optics, *Nature* **541**, 473 (2017).
- [52] H. Zheng, D. J. Gauthier, and H. U. Baranger, Waveguide-QED-Based Photonic Quantum Computation, *Phys. Rev. Lett.* **111**, 090502 (2013).
- [53] Q. Quan, I. Bulu, and M. Lončar, Broadband waveguide qed system on a chip, *Phys. Rev. A* **80**, 011810 (2009).
- [54] J.-T. Shen and S. Fan, Strongly Correlated Two-Photon Transport in a One-Dimensional Waveguide Coupled to a Two-Level System, *Phys. Rev. Lett.* **98**, 153003 (2007).
- [55] C. Lee, C. Noh, N. Schetakis, and D. G. Angelakis, Few-photon transport in many-body photonic systems: A scattering approach, *Phys. Rev. A* **92**, 063817 (2015).
- [56] S. Xu and S. Fan, Input-output formalism for few-photon transport: A systematic treatment beyond two photons, *Phys. Rev. A* **91**, 043845 (2015).
- [57] D. F. Walls and G. J. Milburn, *Quantum Optics* (Springer Science & Business Media, Berlin, 2007).
- [58] A. V. Gorshkov, A. André, M. D. Lukin, and A. S. Sørensen, Photon storage in  $\Lambda$ -type optically dense atomic media. I. cavity model, *Phys. Rev. A* **76**, 033804 (2007).
- [59] L.-M. Duan and H. J. Kimble, Scalable Photonic Quantum Computation through Cavity-Assisted Interactions, *Phys. Rev. Lett.* **92**, 127902 (2004).
- [60] N. H. Lindner and T. Rudolph, Proposal for Pulsed On-Demand Sources of Photonic Cluster State Strings, *Phys. Rev. Lett.* **103**, 113602 (2009).
- [61] J. Zhang, Z. Fang, J. Lin, J. Zhou, M. Wang, R. Wu, R. Gao, and Y. Cheng, Fabrication of crystalline microresonators of high quality factors with a controllable wedge angle on lithium niobate on insulator, *Nanomaterials* **9**, 1218 (2019).
- [62] M. Jazbinsek, L. Mutter, and P. Gunter, Photonic applications with the organic nonlinear optical crystal dast, *IEEE J. Sel. Top. Quantum Electron.* **14**, 1298 (2008).
- [63] A. Majumdar, C. M. Dodson, T. K. Fryett, A. Zhan, S. Buckley, and D. Gerace, Hybrid 2d material nanophotonics: A scalable platform for low-power nonlinear and quantum optics, *ACS Photonics* **2**, 1160 (2015).
- [64] M. Li, L. Zhang, L.-M. Tong, and D.-X. Dai, Hybrid silicon nonlinear photonics [invited], *Photon. Res.* **6**, B13 (2018).
- [65] N. K. Langford, S. Ramelow, R. Prevedel, W. J. Munro, G. J. Milburn, and A. Zeilinger, Efficient quantum computing using coherent photon conversion, *Nature* **478**, 360 (2011).
- [66] E. Timurdogan, C. V. Poulton, M. J. Byrd, and M. R. Watts, Electric field-induced second-order nonlinear optical effects in silicon waveguides, *Nat. Photonics* **11**, 200 (2017).
- [67] M. Heuck, K. Jacobs, and D. R. Englund, Controlled-phase Gate using Dynamically Coupled Cavities and Optical Nonlinearities, arXiv:1909.05751 (2019).